Journal of Power Sources 266 (2014) 99–106

Contents lists available at ScienceDirect

Journal of Power Sources

journal homepage: www.elsevier.com/locate/jpowsour

Stirring effect in hydrothermal synthesis of nano C-$LiFePO_4$

K. Vediappan [a,b], A. Guerfi [a], V. Gariépy [a], G.P. Demopoulos [b], P. Hovington [a], J. Trottier [a], A. Mauger [c], C.M. Julien [d], K. Zaghib [a,*]

[a] Institut de Recherche d'Hydro-Québec (IREQ), 1800 Bd Lionel-Boulet, Varennes, QC J3X 1S1 Canada
[b] Department of Mining and Materials Engineering, McGill University, Montreal, QC H3A 2B2 Canada
[c] Sorbonne Universités, UPMC Univ Paris 06, Institut de Minéralogie, de Physique des Matériaux et de Cosmochimie (IMPMC), 4 place Jussieu, F-75005 Paris, France
[d] Sorbonne Universités, UPMC Univ Paris 06, Physicochimie des Electrolytes et Nanosystèmes Interfaciaux (PHENIX), 4 place Jussieu, F-75005 Paris, France

HIGHLIGHTS

- $LiFePO_4$ cathode depends strongly on the frequency of rotation of the impeller.
- Dependence is attributable to the difference in the agglomeration phenomena in secondary particles.
- The presence of secondary particles of size ≈10 μm is beneficial.

GRAPHICAL ABSTRACT

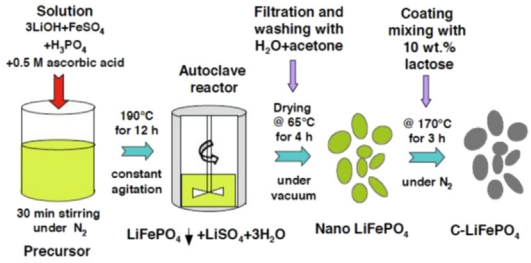

ARTICLE INFO

Article history:
Received 15 January 2014
Received in revised form
1 May 2014
Accepted 2 May 2014
Available online 13 May 2014

Keywords:
Nano C-$LiFePO_4$
Hydrothermal synthesis
Stirring effect
Lithium-ion batteries

ABSTRACT

C-$LiFePO_4$ positive electrode materials were prepared by hydrothermal synthesis in which the solution was stirred with a rotation frequency varying from 50 to 1150 revolutions per minute (rpm), before carbon coating. The different synthesized cathode materials are discussed and compared in terms of structural, surface-morphological and electrochemical properties. The best C-$LiFePO_4$ electrodes have been obtained using rotation frequencies in the range 280–360 rpm, in which case the capacity retention reaches ~137 mAh g^{-1} at coulombic efficiency >99% at C/12, against 106 mAh g^{-1} in the absence of agitation. Better cycling stability at high current rates (1C) were also obtained. The improved performance of the C-$LiFePO_4$ material obtained by controlled rotating agitation-hydrothermal solution synthesis is attributed to the production of less aggregated particles with high surface area and smaller concentrations of impurities. The controlled rotating agitation of the solution during the synthesis provides a scalable and eco-friendly way of producing better performing electrode particles for use in Li-ion batteries.

1. Introduction

$LiFePO_4$ (LFP) first proposed as a positive electrode for lithium-ion batteries by Goodenough [1] offers unique advantages with respect to the lamellar and manganese spinel compounds. Thanks to the strong covalent bonded PO_4 groups and the chemically stable $Fe^{2+/3+}$ redox couple as around 3.45 V, LFP offers better electrochemical stability and cycling life than other electrode active materials [2–7]. Also it has a long cycle life, good rate capability and capacity [3,6]. Today, this material is commercialized as one of the most prominent active materials of Li-ion batteries across the world, in particular for electric and hybrid vehicles [6,7], and it has

* Corresponding author. Tel.: +1 450 652 8019; fax: +450 652 8204.
E-mail address: zaghib.karim@ireq.ca (K. Zaghib).

http://dx.doi.org/10.1016/j.jpowsour.2014.05.005
0378-7753/

been subject to many investigations that have been summarized in different reviews [8,9] and books [10–12]. Nevertheless, the olivine structure in which the material crystallizes implies that the Li path is one-dimensional in nature, so that the Li diffusion is very sensitive to any impurity or defect that would block the Li-channels [13,14]. As a consequence, $LiFePO_4$ must be prepared well crystallized and free of impurity, and many synthesis routes have been explored to fulfill this purpose. They have been reviewed in Refs. [9,15]. Among them, the hydrothermal route presents some advantages [3], including the possibility to control the chemical composition and crystallite size [5,16–28]. This is not the cheapest way to prepare the material, but it can be used to prepare submicron $LiFePO_4$ particles of very good quality [28–34]. However, to meet the increasing demand for C-$LiFePO_4$, the optimization of the different hydrothermal synthesis parameters is needed. In a prior work, we have investigated the effect of the complexing agent used in the hydrothermal synthesis [34]. In the present work, we find that another parameter, namely the rotation frequency ν of the impeller used for the mixing during the synthesis, is also an important parameter to produce C-$LiFePO_4$ electrodes with superior electrochemical performance. In some of the prior works cited above, the mixture of the precursors in the autoclave was not agitated. However, a reactor with impeller is usually preferred because the stirring helps to obtain a uniform mixing and hence better control on the final product with reproducible properties. Aiming to optimize the parameter ν, LFP samples have been synthesized by hydrothermal process using different rotation speeds for the agitator, from 50 up to 1150 revolutions per minute (rpm), before carbon coating. The samples have been characterized by XRD, TEM, FTIR, and the analysis of the magnetic properties. The best electrochemical performance has been obtained for a rotation speed 280 rpm.

2. Experimental details

2.1. Preparation of C-$LiFePO_4$

The hydrothermal synthesis was performed following the procedure described in Fig. 1. The precursor chemicals were $LiOH \cdot H_2O$, $FeSO_4 \cdot 7H_2O$, H_3PO_4 (85 wt.%) and ascorbic acid; the Li, Fe, P, and C were standardized in the molar ratio Li:Fe:P:ascorbic acid = 3:1:1:0.2. The concentration of ascorbic acid was adjusted to obtain pH = 7. The Li source and P source were dissolved in deionized water under magnetic stirring for 30 min until a mass of sticky mixture was formed. Then, $FeSO_4$ and ascorbic acid in aqueous solution were added slowly with continuous stirring. In order to eliminate the oxidation of Fe^{2+} to Fe^{3+}, the water was degassed by N_2 gas bubbling for 30 min prior to preparing the solution. The hydrothermal reactor was a stainless steel autoclave (inner volume: 0.3 dm^{-3}) equipped with a mixing accessory and quartz liner (MMJ-500-HC, OM Labtec Co., Ltd, Japan). The Teflon-lined autoclave was heated to 190 °C for 12 h, during which the solution was stirred at a speed in the range 50–1150 rpm. The precipitated powders were collected by filtration and washed thoroughly with deionized water and acetone. The powders were then dried at 65 °C for 4 h under dry vacuum condition.

The $LiFePO_4$ samples obtained at this step are not carbon-coated. However, carbon coating is mandatory to increase the electronic conductivity powder to be used as the active element of a positive electrode [35]. For this purpose, the powders were mixed with 10 wt.% of lactose solution to provide a carbon source and heat-treated at 700 °C for 3 h under flowing N_2 to form C-$LiFePO_4$ [2,36,37]. We know from these previous works that this temperature is small enough so that the carbon coating process does not modify the size distribution of the particles.

2.2. Characterization

Powders were characterized using X-ray diffraction (XRD) analysis in the 2θ range 10–90° with scan rate of 0.025° min^{-1} on a Philips X'Pert PRO MRD (PW3050) diffractometer equipped with a Co anticathode (CoK_α radiation λ = 0.178897 nm) at room temperature. The FTIR spectroscopy measurements were carried out using a Bruker Vertex 70v ATR (diamond window). The surface morphology and particle size of the samples were observed using a Hitachi (Japan) scanning electron microscope (SEM). The conductivity measurements of as prepared C-LFP samples were done using a powder resistivity measurement system (PRMS) from Loresta-GP.

2.3. Cell construction

The C-$LiFePO_4$ was added to form a suspension consisted of 84 wt.% active electrode powder plus vapor-grown carbon fiber (3 wt.%), super black (3 wt.%) and the binder was polyvinylidene difluoride (PVDF) (10 wt.%) in *N*-methyl-pyrrolidinone. After 10 min grinding with a mortar, the viscous slurry was coated on an aluminum foil, then dried for 24 h at 95 °C in vacuum. The coated electrode was pressed under a 7-ton load to a thickness of about 40 μm, and then punched out to produce 14-mm diameter cathodes. These electrodes were dried at 120 °C for 5 h in a vacuum drying oven. The 2032 coin-type cells (20-mm diameter and 3.2-mm thick) were assembled in a glove box in a high purity argon

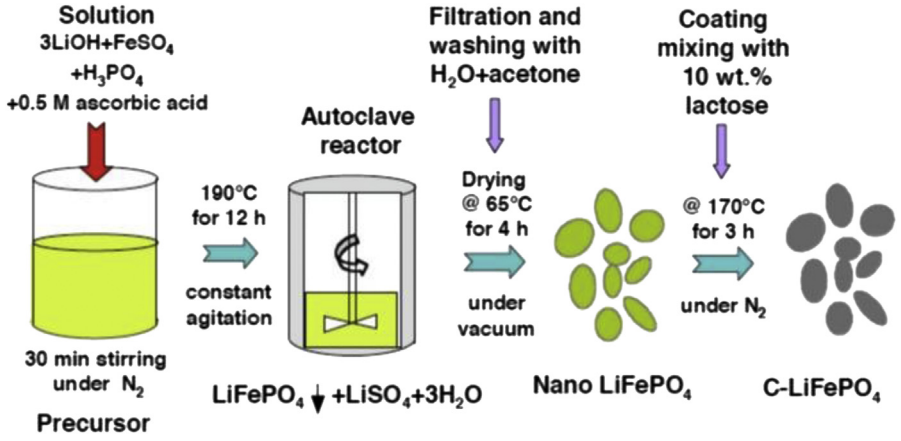

Fig. 1. Schematic representation of the synthesis procedure of LFP particles using a stirring hydrothermal method.

atmosphere. The cell consisted of the cathode, pure metallic Li anode, microporous membrane (Celgard 2400) separator and a non-aqueous electrolyte of 1 mol dm^{-3} $LiPF_6$ in ethylene carbonate (EC): dimethyl carbonate (DMC) (1:1v/v). The cells were cycled at 25 °C between 2.0 and 4.0 V vs. Li^0/Li^+ at constant current on a Mac-Pile battery cycler.

3. Results

3.1. Structural studies

The XRD spectra of the different samples are shown in Fig. 2. In addition to the peaks characteristics of the olivine structure indexed in the figure, small diffraction peaks can be detected at 2θ angles marked by vertical dotted lines in Fig. 2. These additional peaks can be identified as due to Li_3PO_4 impurity at the surface of the particles. This impurity is observed when the synthesis is performed with an excess of Li with respect to the ideal stoichiometry among the precursors [38]. Coating with Li_3PO_4 can be done on purpose since it reduces the resistance of the solid–electrolyte interface [39], but it also acts as an inert mass that reduces the capacity retention [38]. The size of the crystallites was calculated from the XRD line width using the Scherrer's formula, $d = 0.9\lambda/b_{1/2}\cos\theta$, where λ is the X-ray wavelength, $b_{1/2}$ is the corrected width at half-height of the main diffraction peaks, and θ is the diffraction angle. The procedure to determine $b_{1/2}$ has been reported elsewhere [40]. The parameter d has been measured for different angles corresponding to the (200), (101), (111), (211) and (311) lines. No significant dependence on θ has been evidenced. The result is $d = 42 \pm 2$ nm for the samples obtained with $\nu \leq 360$ rpm. On another hand, d is reduced to 30 nm when $\nu = 1150$ nm. This reduced coherence length is the first evidence that this agitation speed is too high to obtain well-crystallized LFP.

The SEM images of the particles are reported in Fig. 3 for the sample prepared at $280 \geq \nu \geq 1150$ rpm. For $\nu = 280$ rpm, the primary particles are elongated spheroids about 300 nm long, while the equatorial diameter is circa 150 nm. That is true for all the samples that have been prepared at $\nu = 360$ rpm. The non-spherical shape of submicron particles was previously observed and explained as a result of the geometry of the olivine structure [41,42]. On another hand, the sample prepared at $\nu = 1150$ rpm shows a different morphology, as it can be seen in Fig. 3. The

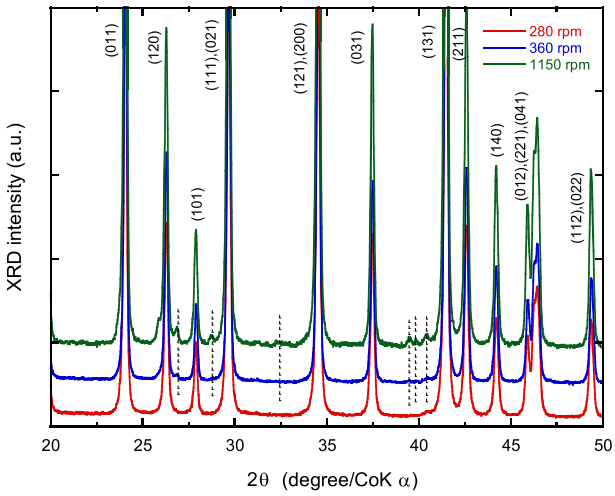

Fig. 2. Details of the XRD spectra in the 2θ-range 20–50° of LFP prepared by hydrothermal synthesis at three different stirring speeds: 280, 360 and 1150 rpm. The vertical broken lines indicate the positions of the peaks associated to the Li_3PO_4 impurity.

particles obtained at this agitation speed are deformed and twice bigger than the particles obtained at lower frequency ν. This is the confirmation of the analysis of the XRD spectra showing that the too strong agitation at 1150 rpm did not allow the precursors to react to form well-crystallized particles. TEM images of primary particle after carbon coating are reported in Fig. 4a–b. The images are the same for the samples obtained at $\nu \leq 360$ rpm so that only the result at the intermediate speed $\nu = 280$ rpm (Fig. 4a) has been reported as an illustration, showing the carbon layer about 2 nm thick covering the well-crystallized surface. On another hand, the surface of the sample at $\nu = 1150$ rpm is irregular and so is the carbon layer, which confirms the stronger disorder at the surface layer (Fig. 4b).

The granulometry of the powder measured with the ParticaLA-950V2 Laser Diffraction Particle Size Analyser (HORIBA Instruments) is reported in Fig. 5. The measurements have been performed before carbon coating (see section 2.1), but we have checked that ithe size distribution remains unchanged after the carbon coating, in agreement with our prior work according to which the shape and size distribution of the particles are not modified at the sintering temperature (700 °C) used in the coating process. All the curves show a first peak at 0.3 μm, which corresponds to the primary particles. There are, however, remarkable differences in the size distribution of the particles at larger values, depending on the parameter ν. For $\nu = 280$ rpm, another maximum at 10 μm gives evidence of a partial aggregation of the primary particles to form secondary particles of diameters distributed around this size. For $\nu = 360$ rpm, the aggregation is much smaller since the integrated peak at 10 μm is larger, and the amount of secondary particles has been reduced. Therefore, when $\nu \geq 280$ rmp, the agitation becomes strong enough to impeach the aggregation of the primary particles. On the other hand, when for $\nu = 50$ rpm, the agitation is too slow to avoid the aggregation that is increased. The amount of isolated primary particle is almost the same as in the case $\nu = 280$ rpm, but the average size of the aggregates is larger, peaking at 200–300 μm.

The FTIR absorption spectrum of the sample prepared at 280 rpm is reported in Fig. 6, together with that of the sample prepared at 50 and 1150 cm^{-1} for comparison, in the high-frequency region 600–1200 cm^{-1} corresponding to the stretching modes of phosphate entities. The spectrum of the samples prepared at $\nu = 360$ rpm is the same as that of 280 rpm and has thus not been reported in the figure. The spectra are characteristics of LFP and have been described in detail elsewhere [43]; the bands have been identified, for instance, in Ref. [44]. The only band that is not an intrinsic property of LFP is the additional structure at 1094 cm^{-1} in Fig. 6. This structure is the signature of the Li_3PO_4 impurity [45] already detected by RXD analysis. On another hand, no structure has been observed in the vicinity of 760 cm^{-1}, which is the wave-number characteristic of the symmetric stretching mode of P_2O_7 pyrophosphate groups. Also, the bands at 942 and 974 cm^{-1} associated to symmetric stretching modes of PO_4 units are barely resolved in the case $\nu = 1150$ rpm, merging in a single broad band centered at 955 cm^{-1}. This is another evidence of the presence of strains and local disorder in this ill-crystallized sample.

To complete the characterization, measurements of the magnetic properties have been made, since they are much more sensitive to the presence of impurities than XRD or even FTIR experiments. The results are the same for all the samples, and reported for one of them in Fig. 7. The magnetization varies linearly with the magnetic field, at any temperature above 5 K, so that the samples are free from any iron-containing impurities like γ-Fe_2O_3, Fe_2P, or $Li_3Fe_2(PO_4)_3$ that can poison $LiFePO_4$ [46,47]. The Curie–Weiss law in the paramagnetic regime is well satisfied; the effective

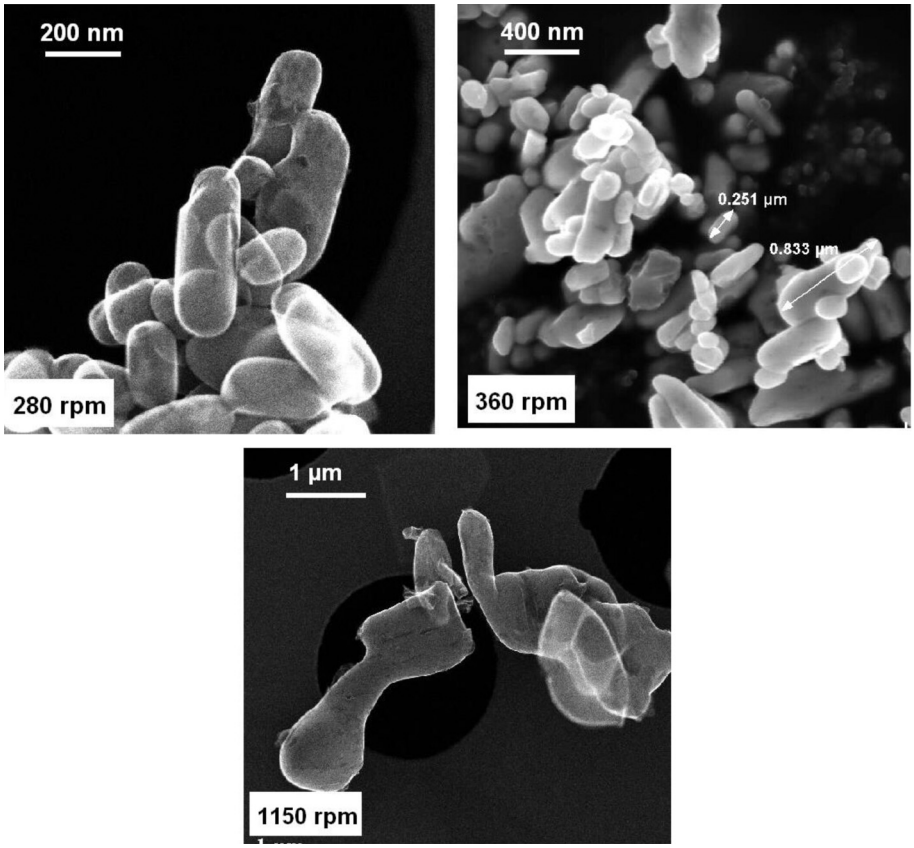

Fig. 3. SEM images of the surface morphology of C-LiFePO$_4$ particles prepared by stirring hydrothermal method at 280, 360 and 1150 rpm speed.

magnetic moment of the iron is 5.47 μ_B, significantly larger than the theoretical value 4.9 μ_B expected for Fe^{2+}. Since, however, the only impurity in the samples is Li_3PO_4 that is not magnetic, we can conclude that this excess of magnetic momentum results from the magnetic polarons associated to Li vacancies [48].

The electrochemical properties of the three samples are illustrated in Fig. 8 where we have reported the voltage–capacity curves measured at 1C-rate. As expected, the capacity of the ill-crystallized sample prepared at 1150 rpm is very small and does not require further comments. The largest capacity and also the smallest difference between charge and discharge curves have been obtained for $\nu = 280$ rpm. Fig. 9 shows that the cell with LFP prepared at 280 rpm does not age upon cycling up to the 120 cycles that have been tested, confirming that 280 rpm is the optimized rotation speed for the preparation of LFP by the hydrothermal route. In addition the cell with LFP prepared at 280 rpm does not age upon cycling up to the 120 cycles that have been tested, confirming that 280 rpm is the optimized rotation speed for the preparation of LFP by the hydrothermal route. The Modified Peukert plot in Fig. 10 shows the superiority of the cell with LFP synthesized under stirring at 280 rpm at any C-rate. The main difference among the samples prepared with $\nu \leq 360$ rpm is between charge and discharge curves of the cells in Fig. 8. This polarization effect is smaller in the cell prepared with $\nu = 280$ rpm, which suggests that this is the value of ν for which the conductivity of the cell is the best.

To verify this conclusion, EIS studies were carried out using a VMP-cycler (Biologic, France), with an ac amplitude of 5 mV in the frequency range of 200 kHz–50 mHz. The results are reported under the form of the Nyquist plot in Fig. 11a. The plot consists of an arc of circle (high-frequency regime) followed by a linear part (low-frequency regime), which can be analyzed separately, since they are well separated. At low frequency, the slope of the linear part is not equal to 45° as expected for the semi-infinite Warburg limit. Such a behavior gives evidence of distributed time constants that may have different causes: a microscopic roughness always present on the surface of the particles, causing a coupling of the solution resistance with the surface capacitance, or a capacitance dispersion of interfacial origin, connected with slow adsorption of ions and chemical inhomogeneity of the surface [49,50]. In the present case, however, where the surface of the C-LiFePO$_4$ prepared at $\nu \leq 360$ rpm are well-crystallized, the origin of the broad dispersion of relaxation time is linked to the separation between primary and secondary particles. In such cases the complex impedance is expressed in terms of a so-called constant phase element, CPE. Its impedance is given by:

$$Z_{CPE} = \frac{1}{\sigma(j\omega)^{\phi}}, \quad (1)$$

where σ is a constant, and ϕ is related to the angle of rotation of a purely capacitive line on the complex plane plots: $\alpha = 90\infty(1-\phi)$. This equation can also be written:

$$Z_{CPE} = \frac{1}{\sigma\omega^{\phi}}[\cos(\pi\phi/2) - j\sin(\pi\phi/2)]. \quad (2)$$

It represents a “leaking” capacitor, which has non-zero real and imaginary components. Therefore, at low frequency, the electrode impedance may be expressed as a sum of the resistance R and the impedance of the CPE element:

$$Z = R + Z_{CPE}. \quad (3)$$

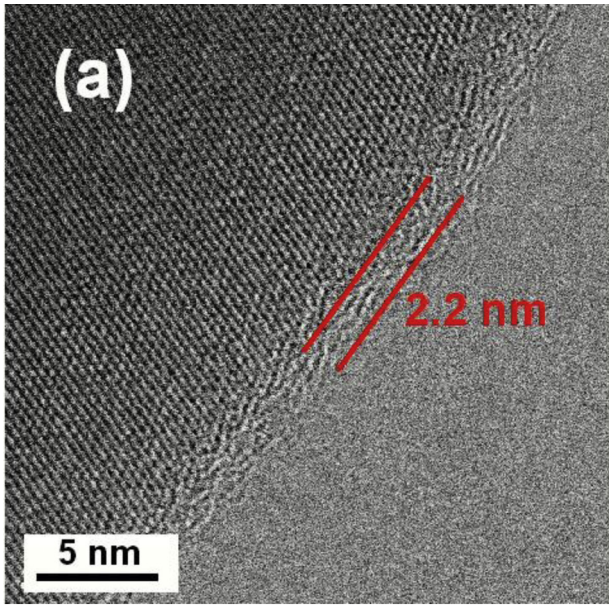

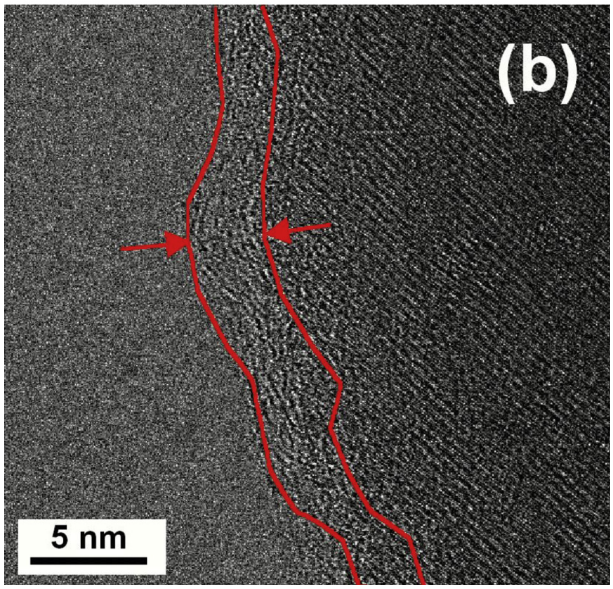

Fig. 4. TEM images of the surface morphology of C-$LiFePO_4$ particles prepared by hydrothermal method at $\nu = 280$ rpm (same images are obtained at 360 rpm) and 1150 rpm stirring speed. The contour of the carbon layer is marked in full curve when it is well defined, but only as a broken line at the interface with the LFP particle for the 1150 rpm case, since the interface is not well defined because of some disorder in the surface layer.

The slope of the linear part in Fig. 11a gives $\phi = 0.84$ for the electrodes equipped with the powders prepared at 280 and 320 rpm. This value of ϕ is intermediate between the semi-infinite Warburg limit $\phi = 0.5$, and the purely capacitive behavior $\phi = 1$, as expected. The two electrodes differ only by the value of the resistance $R = 111$ and 156 Ω with LFP prepared at 280 and 360 rpm, respectively.

At high frequency, the complex impedance deviates from the ideally polarizable electrode case, and is dominated by the Faradaic reaction. Due to the CPE term, the impedance should be an arc of circle, but in the present case, this arc is flattened and it is the superposition of two arcs. To better understand this effect of the distribution of relaxation times, we have reported in Fig. 11b the Bode plot of $-Z'' = -\mathrm{Im}(Z)$ as a function of the frequency in the logarithmic scale. These curves go through a secondary maximum. In the

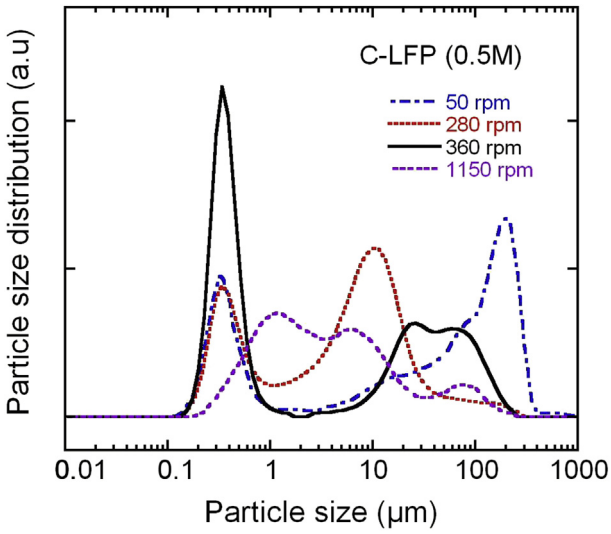

Fig. 5. Distribution size of C-$LiFePO_4$ particles prepared by hydrothermal method at different stirring speed. Data show clearly the size of primary particles (first peak at 300 nm) and that of agglomerates at larger sizes.

case $\nu = 360$ rpm, the curve is approximately symmetric on both sides of this extremum, as expected for a Gaussian distribution of relaxation times. For the case $\nu = 280$ rpm, however, this symmetry is lost, and the curve can be de-convoluted in two Gaussians, centered on frequencies f indicated by the vertical arrows in Fig. 11a, and converted in relaxation time $\tau = 1/f$ in Fig. 11b. The Gaussian centered at lower frequencies is attributable to the activity of the secondary particles, and is not observed with the sample prepared at $\nu = 380$ rpm because there are almost no secondary particles in this case. The same analysis is reported in the figures for the case $\nu = 1150$ rpm, showing that the characteristic relaxation times are shifted by one order of magnitude toward longer relaxation times, which again gives evidence of the low conductivity that prevents any fast motion of electrons and ions in this case.

4. Discussion

The poor electrochemical properties obtained when $\nu = 1150$ rpm are due to the fact that the LFP sample was ill-

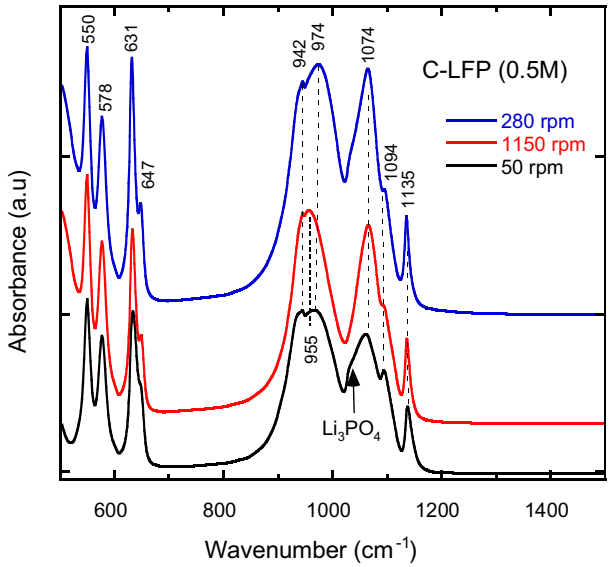

Fig. 6. FTIR spectra of $LiFePO_4$ obtained at $\nu = 50$, 280 and 360 rpm stirring speed.

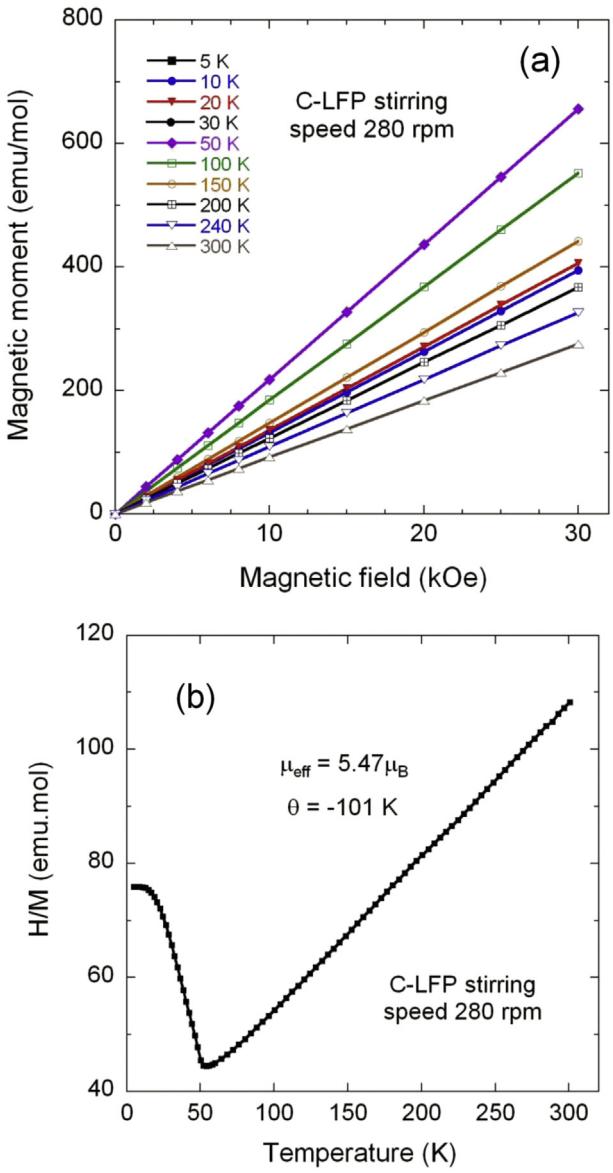

Fig. 7. (a) Isothermal plots of the magnetic moment *vs.* magnetic field and (b) temperature dependence of M/H for a C-$LiFePO_4$ sample prepared at 280 rpm stirring speed.

crystallized due to this too strong stirring. One can also invoke the fact that irregular particle morphology reduces the electrochemical performance. This has been evidenced in $LiMn_2O_4$ [51], and we find the same result here. In addition, we find that this irregular shape is actually the consequence of the ill-crystallization, which is presumably a more important factor than the geometrical shape of the particles to explain the poor electrochemical performance. The rotation frequency has thus an effect on the nucleation/growth kinetics when the rotation speed is too large ($\nu = 1150$ rpm), by preventing the crystal growth. In the frequency range of interest ($\nu \leq 360$ rpm), however, the rotation has no effect on the nucleation/growth kinetics, which is evidenced by the fact that the shape and size of the primary particles are independent on ν''. The discussion will then be focussed on these other samples prepared at $\nu \leq 360$ rpm. They are free from any impurity except Li_3PO_4. This impurity acts as an inert mass, so that its only effect is to decrease the initial capacity with respect to the theoretical one. However, the impurity peaks in the XRD spectra have roughly the same amplitude, and the impurity band in FTIR spectra also has the same amplitude, so that the amount of Li_3PO_4 can be considered as identical in the samples. Therefore, the difference in the electrochemical difference among the other samples is entirely attributable to the difference in the agglomeration phenomena in secondary particles. Although the agglomeration of active positive electrodes impacts the electrochemical properties of Li-ion batteries, its effect has been rarely investigated in the past [51] and most of the attention has been focussed on tailoring the size of the primary particles [52]. The comparison of the results obtained between the samples prepared at $\nu \leq 360$ rpm gives us the opportunity to learn more about the agglomeration effect, since the powders have the same primary particles. For $\nu = 50$ rpm, the fraction of the primary particles that are not involved in agglomerates is the same as in the case $\nu = 280$ rpm. The difference is that the agitation at $\nu = 50$ rpm is too slow so that the mixing does not prevent the formation of big agglomerates, the average size of which is about 200–300 μm. This large size is responsible for the degradation of the electrochemical properties, presumably because the electrolyte has more difficulties to penetrate the core region of the secondary particles so that the ionic conductivity is lowered. On another hand, the average size of the secondary particles is reduced to 10 μm. This size is small enough to let the electrolyte penetrate in the core region of the secondary particles. Therefore, the formation of these agglomerates increases the compactness without altering the electrochemical performance. On another hand, at $\nu = 360$ rpm, the agitation is fast enough to avoid the formation of most of the secondary particles. Nevertheless, the electrochemical performance is smaller than in the case $\nu = 280$ rpm. Indeed, the configuration of isolated primary particles optimizes the surface area in contact with the electrolyte, but it is also the configuration where side reactions can take place between the electrode and the electrolyte, with the formation of a passivation layer on the electrode resulting in larger polarization of the cell.

The optimal rotation speed is 280 rpm in the present work, but it is specific to the shape and size of the particles. The hydrothermal process is known to make possible the preparation of primary particles of different shape and different sizes, depending on the synthesis conditions. The solid-state synthesis process allows for the synthesis of more spherical primary particles. Therefore, a multi-factor engineering research is now needed to determine the optimal stirring as a function of the shape and size of the primary particles that can be prepared, depending on the applications that are envisioned. In the present work, we have chosen a synthesis process (hydrothermal), that guarantees the formation of well-crystallized particles, and synthesis conditions that give primary particles of a size (circa 300 nm) that are currently prepared in the industry. Another advantage of the choice of this size of primary particles is that it avoids the disorder of the surface layer that is favored by the decrease of the size of the particles below 50 nm (for a review of surface effects in $LiFePO_4$, see Ref. [9]). For the particle size used in the present work, we have shown that the carbon coating process used in the present work results in the re-crystallization of the surface layer [37]. In particular, it prevents the formation of pores, thus avoiding the introduction of the porosity as an additional parameter. Note also that the carbon coating is made as a second step after the hydrothermal synthesis, which guarantees that the carbon coating and the electronic conductivity is identical for all the samples, irrespective of the stirring speed used during the hydrothermal synthesis, thus avoiding the introduction of the electric conductivity as an additional parameter. The stirring parameter (rotation speed) is thus the only parameter that is pertinent to explain the difference in the electrochemical

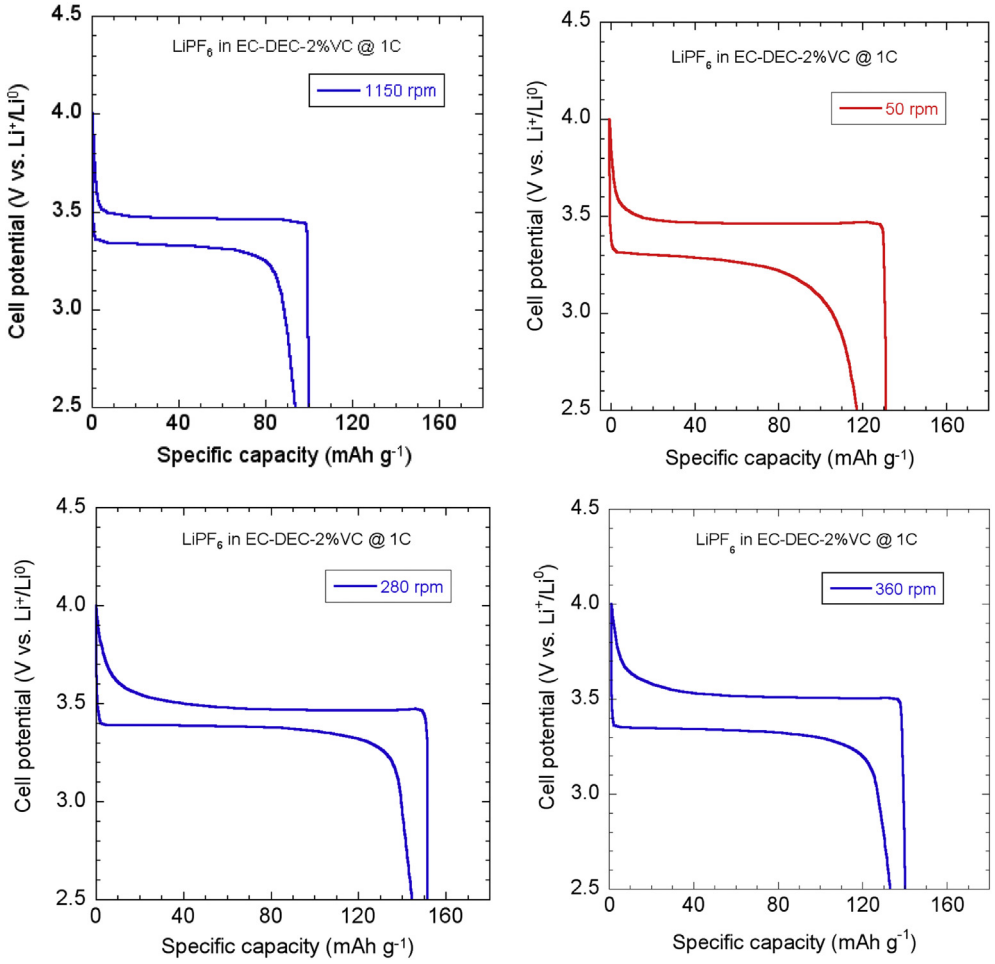

Fig. 8. Electrochemical profiles of C-$LiFePO_4$//Li coin cells as a function of the stirring speed ν = 280, 360 and 1150 rpm. Charge-discharge cycles were carried out at 1C in the 2.5–4.5 V potential range.

properties between the different samples we have investigated. We can thus conclude that the stirring is the key parameter responsible for the formation of the secondary particles that impact the electrochemical properties in the present work.

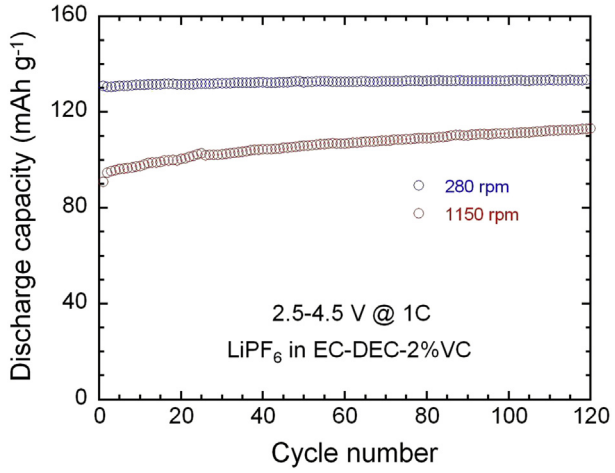

Fig. 9. Discharge capacity of Li//C-$LiFePO_4$ cells as a function of the cycle number for positive electrodes synthesized at different stirring speeds. Data were collected at 1C in the 2.5–4.5 V potential range.

5. Conclusion

$LiFePO_4$ powders with primary particles of average size 300 nm have been prepared by hydrothermal process. The speed of the rotating agitator in the reactor is an important parameter that dictates the formation of secondary particles. We found that the

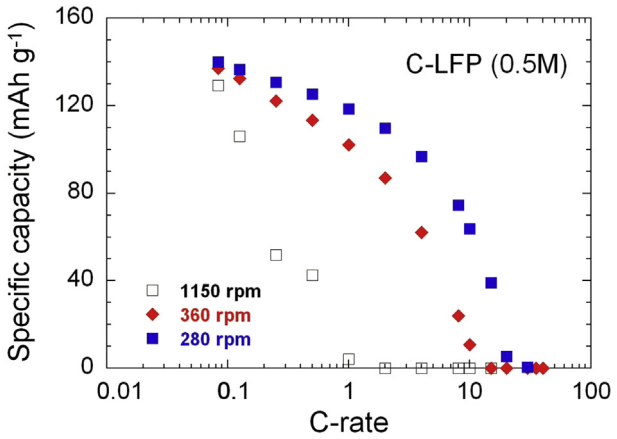

Fig. 10. Modified Peukert plot for the Li//C-$LiFePO_4$ coin cells with positive electrodes synthesized at ν = 280, 360 and 1150 rpm stirring speed.

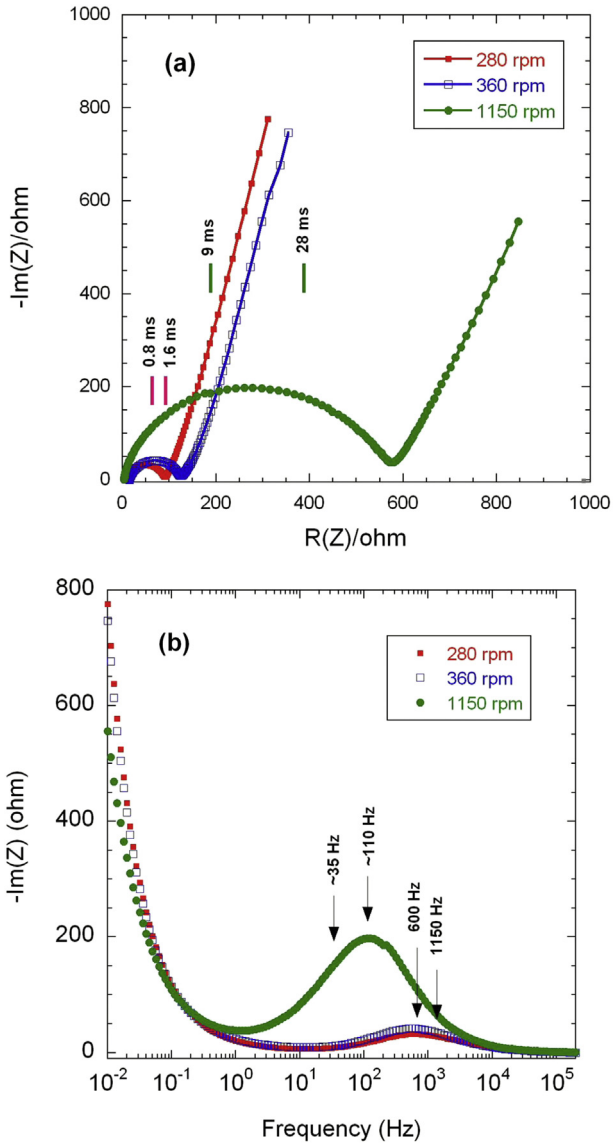

Fig. 11. (a) Nyquist plot of the EIS data showing the $-\mathrm{Im}(Z)$ as a function of $\mathrm{Re}(Z)$. (b) Bole plot of $-\mathrm{Im}(Z)$ versus the frequency. The vertical lines show the frequencies f (curves a) or the relaxation times $1/f$ (curves b) corresponding to the secondary maxima of the two Gaussian coming from the de-convolution of the Bole plots at 360 and 1150 rpm.

stirring at 280 rpm is the best speed to obtain a powder that optimizes the electrochemical properties. This speed realizes the best compromise as it is large enough to allow the formation of small agglomerates (average size: 10 μm) that minimizes the side reactions with the electrolyte while insuring a large surface area.

References

[1] A.K. Padhi, K.S. Nanjundaswamy, J.B. Goodenough, J. Electrochem. Soc. 144 (1997) 1188.
[2] K. Zaghib, A. Guerfi, P. Hovington, A. Vijh, M. Trudeau, A. Mauger, J.B. Goodenough, C.M. Julien, J. Power Sources 232 (2013) 357.
[3] J. Chen, Recent Pat. Nanotech 7 (2013) 2.
[4] X. Li, F. Kang, X. Bai, W. Shen, Electrochem. Commun. 9 (2007) 663.
[5] K. Dokko, K. Shiraishi, K. Kanamura, J. Electrochem. Soc. 152 (2005) A2199.
[6] K. Zaghib, M. Dontigny, A. Guerfy, P. Charest, I. Rodrigues, A. Mauger, C.M. Julien, J. Power Sources 196 (2011) 3949.
[7] K. Zaghib, J. Dubé, A. Dallaire, K. Galoustov, A. Guerfi, M. Ramanathan, A. Benmayza, J. Prakash, A. Mauger, C.M. Julien, J. Power Sources 219 (2012) 36.
[8] K. Zaghib, A. Mauger, C.M. Julien, J. Solid State Electrochem 16 (2012) 835.
[9] C.M. Julien, A. Mauger, K. Zaghib, J. Mater. Chem. 21 (2011) 9955.
[10] K. Zaghib, A. Mauger, J.B. Goodenough, F. Gendron, C.M Julien, in: J. Garche (Ed.) 5 vols., Elsevier Science, 2009.
[11] K. Zaghib, A. Mauger, J. Goodenough, C.M. Julien, in: D. Lockwood (Ed.), Nanotechnology for Li-ion Batteries, Springer Verlag, Berlin, 2011 (Chapter 8).
[12] K. Zaghib, J. Dubé, A. Dallaire, K. Galoustov, A. Guerfi, M. Ramanathan, A. Benmayza, J. Prakash, A. Mauger, C.M. Julien, Handbook on Lithium-Ion Battery Applications, Elsevier, 2013.
[13] T. Maxisch, F. Zhou, G. Ceder, Phys. Rev. B 73 (2006) 104301.
[14] M.S. Islam, D.J. Driscoll, C.A. Fischer, P.R. Slater, Chem. Mater. 17 (2005) 5085.
[15] O. Toprakci, H.A.K. Toprakci, L. Ji, X. Zhang, Kona Powder Part. J. 28 (2010) 50.
[16] J. Chen, M.S. Whittingham, Electrochem. Commun. 8 (2006) 855.
[17] S. Yang, P.Y. Zavajil, M.S. Whittingham, Electrochem. Commun. 3 (2001) 505.
[18] A.V. Murugan, T. Muraliganth, A. Manthiram, J. Electrochem. Soc. 156 (2009) A79.
[19] G. Meligrana, C. Gerbaldi, N. Penazzi, J. Power Sources 160 (2006) 516.
[20] K. Shiraishi, K. Dokko, K. Kanamura, J. Power Sources 146 (2005) 555.
[21] S. Franger, F. Le Cras, C. Bourbon, H. Rouanlt, J. Power Sources 119–121 (2003) 252.
[22] S. Tajimi, Y. Ikeda, K. Uematsu, K. Toda, M. Sato, Solid State Ionics 175 (2004) 287.
[23] J. Lee, A.S. Teja, Mater. Lett. 60 (2006) 2105.
[24] K. Dokko, S. Koizumi, K. Sharaishi, K. Kananura, J. Power Sources 165 (2007) 656.
[25] B. Jin, H.-B. Gu, Solid State Ionics 178 (2008) 1907.
[26] E.M. Jin, B. Jin, D.-K. Jun, K.-H. Park, H.-B. Gu, K.-W. Kim, J. Power Sources 178 (2008) 801.
[27] J. Chen, M.J. Vacchio, S. Wang, N. Chernova, P. Zavajil, M.S. Whittingham, Solid State Ionics 178 (2008) 1676.
[28] J.K. Kim, G. Cheruvally, J.W. Choi, J.U. Kim, J.H. Ahn, G.B. Cho, K.W. Kim, H.J. Ahn, J. Power Sources 166 (2007) 211.
[29] H.C. Shin, W.I. Cho, H. Jang, J. Power Sources 159 (2006) 1383.
[30] H. Shu, X. Wang, Q. Wu, L. Liu, Q. Liang, S. Yang, B. Ju, X. Yang, X. Zhang, Y. Wang, Q. Wei, B. Hu, Y. Liao, H. Jiang, Electrochim. Acta 76 (2012) 120.
[31] A. Yamada, S.C. Chung, K. Hinokuma, J. Electrochem Soc. 148 (2001) A224.
[32] K. Zaghib, P. Charest, M. Dontigny, A. Guerfy, M. Lagacé, A. Mauger, M. Kopek, C.M. Julien, J. Power Sources 195 (2010) 8280.
[33] K. Zaghib, A. Mauger, F. Gendron, C.M. Julien, Ionics 14 (2008) 271.
[34] F. Brochu, A. Guerfi, J. Trottier, M. Kopec, A. Mauger, H. Groult, C.M. Julien, K. Zaghib, J. Power Sources 214 (2012) 1.
[35] N. Ravet, S. Besner, M. Simoneau, A. Vallée, M. Armand, J.F. Magnan, US Patent 6,962,666 (2005).
[36] C.M. Julien, A. Mauger, A. Ait-Salah, M. Massot, F. Gendron, K. Zaghib, Ionics 13 (2007) 395.
[37] M.L. Trudeau, D. Laul, R. Veillette, A.M. Serventi, K. Zaghib, A. Mauger, C.M. Julien, J. Power Sources 196 (2011) 7383.
[38] P. Axmann, C. Stinner, M. Wohlfahrt-Mehrens, A. Mauger, F. Gendron, C.M. Julien, Chem. Mater. 21 (2001) 1636.
[39] S.-X. Zhao, H. Ding, Y.-C. Wang, B.-H. Li, C.-W. Nan, J. Alloys Compd. 566 (2013) 206.
[40] N. Amdouni, K. Zaghib, F. Gendron, C.M. Julien, Ionics 12 (2006) 117.
[41] G. Chen, X. Song, T.J. Richardson, J. Electrochem. Soc. 154 (2007) A627.
[42] T.J. Richardson, in: Proceedings of the Third Annual Conference on Lithium Mobile Power Advances in Lithium Battery Technologies for Mobile Applications, San Diego, USA, 2007.
[43] M.T. Paques-Ledent, P. Tarte, Spectrochim. Acta A 30 (1974) 673.
[44] C.M. Burma, R. Frech, J. Electrochem. Soc. 151 (2004) 1032.
[45] C.M. Julien, K. Zaghib, A. Mauger, H. Groult, Adv. Chem. Eng. Sci. 2 (2012) 321.
[46] A. Ait-Salah, A. Mauger, C.M. Julien, F. Gendron, Mater. Sci. Eng. B 129 (2006) 232.
[47] N. Ravet, M. Gauthier, K. Zaghib, A. Mauger, J. Goodenough, F. Gendron, C. Julien, Chem. Mater. 19 (2007) 2595.
[48] K. Zaghib, A. Mauger, J. Goodenough, F. Gendron, C.M. Julien, Chem. Mater. 19 (2007) 3740.
[49] T. Pajkossy, J. Electroanal. Chem. 364 (1994) 111.
[50] G.J. Brug, A.L.G. van den Eeden, M. Sluyters-Rehbach, J.H. Sluyters, J. Electroanal. Chem. 176 (1984) 275.
[51] H. Huang, C.H. Chen, R.C. Perego, E.M. Kelder, L. Chen, J. Schoonman, W.J. Weydanz, D.W. Nielsen, Solid State Ionics 127 (2000) 31.
[52] J. Li, C. Daniel, D. Wood, J. Power Sources 196 (2011) 2452.